



The interrelationship of dopamine D2-like receptor availability in striatal and extrastriatal brain regions in healthy humans: A principal component analysis of [¹⁸F]fallypride binding

David H. Zald ^{a,b,*}, Neil D. Woodward ^b, Ronald L. Cowan ^b, Patrizia Riccardi ^d, M. Sib Ansari ^c, Ronald M. Baldwin ^c, Ronald L. Cowan ^b, Clarence E. Smith ^c, Helene Hakyemez ^e, Rui Li ^c, Robert M. Kessler ^c

^a Department of Psychology, Vanderbilt University, 325 Wilson Hall, 111 21st Ave. South, Nashville, TN 37212, USA

^b Department of Psychiatry, Vanderbilt University, Nashville, TN, USA

^c Department of Radiology, Vanderbilt University, Nashville, TN, USA

^d Department of Nuclear Medicine, Albert Einstein College of Medicine, Bronx, NY, USA

^e Neuroscience Program, McGill University, Montreal, QC, Canada

ARTICLE INFO

Article history:

Received 11 September 2009

Revised 31 January 2010

Accepted 3 February 2010

Available online 10 February 2010

ABSTRACT

Individual differences in dopamine D2-like receptor availability arise across all brain regions expressing D2-like receptors. However, the interrelationships in receptor availability across brain regions are poorly understood. To address this issue, we examined the relationship between D2-like binding potential (BP_{ND}) across striatal and extrastriatal regions in a sample of healthy participants. PET imaging was performed with the high affinity D2/D3 ligand [¹⁸F]fallypride in 45 participants. BP_{ND} images were submitted to voxel-wise principal component analysis to determine the pattern of associations across brain regions. Individual differences in D2-like BP_{ND} were explained by three distinguishable components. A single component explained almost all of the variance within the striatum, indicating that individual differences in receptor availability vary in a homogenous manner across the caudate, putamen, and ventral striatum. Cortical BP_{ND} was only modestly related to striatal BP_{ND} and mostly loaded on a distinct component. After controlling for the general level of cortical D2-like BP_{ND} , an inverse relationship emerged between receptor availability in the striatum and the ventral temporal and ventromedial frontal cortices, suggesting possible cross-regulation of D2-like receptors in these regions. The analysis additionally revealed evidence of: (1) a distinct component involving the midbrain and limbic areas; (2) a dissociation between BP_{ND} in the medial and lateral temporal regions; and (3) a dissociation between BP_{ND} in the medial/midline and lateral thalamus. In summary, individual differences in D2-like receptor availability reflect several distinct patterns. This conclusion has significant implications for neuropsychiatric models that posit global or regionally specific relationships between dopaminergic tone and behavior.

© 2010 Elsevier Inc. All rights reserved.

Introduction

Dopamine (DA) is implicated in neuropsychiatric disorders ranging from Parkinson's disease to schizophrenia and addiction (Seeman et al., 1987; Thobois et al., 2004; Wise, 1996). Neurobehavioral theories of DA's role in psychopathology range from relatively global models of hyper- or hypo-dopaminergic tone to complex interactive models, such as those for schizophrenia, which posit a combination of subcortical hyper-dopaminergia and cortical hypo-dopaminergia (Weinberger, 1987). Unfortunately, these models are constrained by current limitations in our understanding of the relationship between DA functioning in different areas of the brain.

As the primary target of DA, DA receptor levels are a key determinant of DA functioning in different brain regions. DA D2-like receptors are widely expressed throughout the brain, with the highest levels in the striatum and moderate levels in the thalamus, hypothalamus, amygdala, hippocampus, and midbrain (Farde et al., 1997; Hall et al., 1996; Kessler et al., 1993; Mukherjee et al., 2002; Rieck et al., 2004). Cortical areas possess substantially lower, but regionally specific levels of D2-like binding, with the highest levels of receptor availability arising in temporal cortices (Olsson et al., 1999). However, the relationship between D2-like receptor levels in cortical and subcortical areas remains poorly understood. The lack of data on this topic results from the simple fact that most D2-like ligands cannot provide stable estimates of both striatal and cortical D2-like levels due to the dramatic differences in DA D2-like receptor density across brain regions. For instance, [¹¹C]raclopride, the most widely used D2-like ligand in PET research, provides stable estimates of D2-like receptor

* Corresponding author. Fax: +1 615 343 8449.

E-mail address: david.zald@vanderbilt.edu (D.H. Zald).

availability in the striatum but does not bind with high enough affinity to measure cortical binding. Other ligands permit measurement of extrastriatal D2-like levels but do not allow stable estimates of striatal binding. The lack of simultaneous assessments has led neurobehavioral theorists to often treat individual differences in striatal D2-like binding as a proxy for D2-like functioning throughout the brain. However, this extrapolation is based on an untested assumption that individual differences in striatal binding are predictive of binding elsewhere in the brain. Moreover, multiple lines of evidence suggest that individual differences in D2-like receptor availability may be heterogeneously expressed across brain regions. The midbrain DA system, which projects to a broad range of cortical and subcortical structures, can be functionally divided into at least three distinct subsystems, typically labeled as the nigrostriatal, the mesocortical, and the mesolimbic systems (Gardner and Ashby, 2000). These systems differ in terms of the topographical origin of DA projection neurons (substantia nigra vs. ventral tegmental area, or dorsal tier vs. ventral tier), as well as a host of electrophysiological, chemical, and functional features that may lead to differential expression of DA receptors (Lewis et al., 2001; Bannon and Roth, 1983; Garris and Wightman, 1994; Tzschentke, 2001; Williams and Goldman-Rakic, 1998). Given the magnitude of these differences, it seems reasonable to speculate that D2-like receptors are differentially regulated in these distinct DA projection systems.

In order to assess the relationship between D2-like receptors in different brain regions, we scanned 45 healthy adult human participants with PET after infusion of the high affinity D2/D3 ligand [¹⁸F]fallypride. Unlike other D2-like ligands, [¹⁸F]fallypride allows stable estimation of both striatal and extrastriatal receptor availability (as indexed by binding potential nondisplaceable BP_{ND}) within a single study session. In order to define the spatial organization of individual differences in D2-like BP_{ND}, we analyzed the data with a voxel-wise principal component analysis (PCA). As applied here, the PCA technique allows determination of which brain areas are associated with each other in their expression of D2-like receptor availability. The PCA approach thus provides an index of the extent to which D2-like receptor availability in different brain regions share a common influence (either functional or methodological) and as such provides a direct assessment of the regional generalizability or specificity of measured individual differences in D2-like functioning.

Materials and methods

Participants

Forty-five healthy participants (22 females and 23 males), all but two of whom were right-handed, participated in the study. The average age was 24.4 years, range 18–44 (the age distribution was skewed in that only 5 subjects were over 30). Female subjects were studied within the first 10 days of their menstrual cycles (menstrual–early follicular phase). All subjects completed written informed consent approved by the Vanderbilt University Institutional Review Board. Subjects received a physical and neurological examination, Structured Clinical Interview for DSM-IV (First et al., 1997), blood chemistry, urine analysis, and urine drug screen in order to ensure that they met all inclusion criteria. Exclusion criteria included a history of psychiatric or neurological condition, use of psychotropic medication in the last 6 months, a history of substance abuse or dependence, current nicotine use or a history of significant nicotine use, major current or past medical illness, and current pregnancy or lactation.

PET imaging and analysis

PET studies were performed on a GE Discovery LS PET scanner using a 3-D emission acquisition. Serial scans were initiated simultaneously with a 30-s bolus infusion of 5.0 mCi [¹⁸F]fallypride

(mean 5.11 mCi, S.D. 0.22 mCi; specific activity >5000 Ci/mmol, mean = 12,345 Ci/mmol, S.D. = 5547 Ci/mmol). Scans of increasing length were obtained for 3.5-h post-infusion. The extended scanning time allowed for stable kinetic model fits in both extrastriatal and striatal brain regions. Participants were given two breaks in scanning in order to avoid fatigue. Following both breaks participants were repositioned using facial markers and given an additional transmission scan for attenuation correction. In order to minimize potential modeling errors due to head motion within and between scans, serial PET scans were coregistered using a mutual information rigid body algorithm (Maes et al., 1997; Wells et al., 1996). Images were reconstructed using a 3-D reprojection algorithm (Kinahan and Rogers, 1989), followed by filtered back projection with correction for scatter and randoms. Parametric images of BP_{ND} were calculated using the full (four-parameter) reference region method (Lammertsma et al., 1996) with the cerebellum used as the reference region, and incorporating all time points into the parameter calculations. Sample time activity curves and model fit lines for several regions are provided in Supplementary Fig. 1. Previous work has demonstrated good test-retest reliability of [¹⁸F]fallypride measurements of BP_{ND} (Mukherjee et al., 2002), and strong correspondence between BP_{ND} as measured by the reference region method, and estimates from metabolite corrected plasma input functions (Kessler et al., 2000). Importantly, the high level of specific activity of the administered [¹⁸F]fallypride and the correction for nonspecific activity provided by the reference region method allow for stable estimates of BP_{ND} that are unaffected by slight variations in dosing or variations in specific activity (see online supporting materials), which is a critical attribute for analyses examining individual differences.

Subjects additionally received an MRI scan using a GE 1.5 T scanner. High resolution, T1-weighted coronal and sagittal IR SPGR sequences were obtained (TE = 3.6, TR = 18.9, TI = 400, slice thickness of 1.2–1.4 mm). PET and MRI scans were coregistered to each other using a mutual information rigid body algorithm (Maes et al., 1997; Wells et al., 1996), with interpolated PET data resampled at 1 mm³. A composite MRI/PET (Pluim et al., 2001) was then created and warped to a common space, using an elastic deformation algorithm (Rhode et al., 2003), and the transformation was applied to the PET BP_{ND} image. For the common space, we utilized a single subject for whom we have both MRI and PET data, and whose brain is approximately the same size as MNI space, although with slightly less asymmetry than the Colin brain included with the SPM5 software. Because of the availability of PET data from this subject, it provides additional information that can be used when aligning composite PET/MRI images. Finally, the warped BP_{ND} images were resampled to 4 mm³ to correspond more closely to the native resolution of the PET camera. In order to maximize the ability to observe differences in nearby structures, no additional spatial smoothing was applied. The global smoothness of the final analyses was 7.1, 8.1, and 8.5 mm full-width half-maximum in the x, y, and z planes, respectively [calculated from residuals in SPM5 (Wellcome Trust Centre for Neuroimaging, London, see Kiebel et al., 1999 for details)]. It may be noted that a greater amount of the variance might have been explained with increased smoothing, but this would come at the expense of detecting differences in neighboring areas.

Principal component analysis

We used a voxel-wise PCA to analyze the data. This data reduction approach analyzes covariance between each voxel in the brain image, in order to derive components that optimally explain the variance across all voxels. The extraction of principal components amounts to a variance maximizing (varimax) rotation of the original variables, such that the first component is the linear combination of the original variables that contributes the most to their total variance. The basic concept of PCA dates back to the early work of Pearson (1901) and

Hotelling (1933) and has been widely applied in image processing (Gonzalez & Woods, 1992; Friston et al., 1993). The extension of the PCA technique to voxel-wise data simply entails a larger covariance matrix and increased computational time compared to applying the technique to a more restricted data set of predefined ROIs. However, it has an advantage over an ROI approach in that the arising components are not constrained by a priori ROI definitions that may not match the actual distribution of covariance throughout brain regions. The PCA was implemented with PCA_image (Keith Worsley, McGill University, Montreal, CN, 2002) coded in MATLAB (Mathworks, Natick, MA, USA).

The data were submitted to the PCA in two formats. In an initial analysis the data were submitted as BP_{ND} maps. However, because the BP_{ND} values and their associated variance are so much higher in the striatum than in other regions, this limits the ability of the PCA to detect components involving nonstriatal regions. We therefore performed a second PCA in which all data were z-transformed, such that each voxel was expressed in terms of the number of standard deviations above or below the 45 participants' mean value for that voxel. Thus, rather than reflecting an absolute value, each subject's z-transformed data reflected the degree to which they had higher or lower than average BP_{ND} at each voxel in the brain. Such an analysis will emphasize components that explain spatially broad areas of covariance. In order to limit the effects of noise in areas with low levels of [^{18}F]fallypride BP_{ND} , data were first masked to only include areas in which subjects on average demonstrated a BP_{ND} of >0.4 (see Fig. 1).

Only components receiving an eigenvalue ≥ 2 are reported (in this context eigenvalues provide a metric of the amount of variance explained by the specific component). Voxel-wise component loadings are expressed from -1 to 1 , where 1 indicates a perfect positive relationship between BP_{ND} and the derived component (i.e., the component fully explains the variance at that voxel), values close to

zero indicate that the variance at the voxel is not explained by the component, and negative values indicate that BP_{ND} in the voxel is inversely related to the component (i.e., BP_{ND} is lower in the region among participants who score high on the component). Overlay of BP_{ND} and PCA loadings on MRI slices and surface renderings were produced with the MRIcro image display program (Chris Rorden, University of Nottingham, UK).

ROI correlation analysis

We additionally provide a correlation analysis of key ROIs. For consistency in definition, ROIs were drawn on an MRI warped to the same common space as the aligned PET images. Because there was no evidence for differential relationships between right and left hemisphere structures, all ROIs were averaged across hemispheres. A priori ROIs included the dorsal striatum (caudate and putamen), ventral striatum, amygdala, hippocampus, and substantia nigra/ventral tegmental area.

For the striatal ROIs, the dorsal caudate and dorsal putamen ROIs were defined by separately tracing the outline of the caudate and putamen on axial slices of the template MRI. In order to avoid possible partial volume effects at the borders of the striatum, tracings were drawn conservatively, such that voxels at the boundary of the striatum (for instance along the boundary with the internal or external capsule) were excluded. To ensure spatial separation from the ventral striatal ROI, the dorsal caudate ROI was limited to slices at and above $z=8$, and the dorsal putamen ROI was limited to slices at and above $z=4$ using Talairach coordinates (see Supplementary Fig. 2). Although, this approach reduces the overall number of voxels included in the caudate and putamen, we selected these more restricted ROIs in order to reduce the degree to which regions near the boundaries of the ROIs could contribute to both ROIs (due to their point spread function), which might heighten the magnitude of correlations between regions. The ventral striatal ROI was drawn on coronal slices from Talairach coordinates $y=+4$ to $+15$. The posterior-most sections of the ventral striatum were excluded from this ROI to limit possible partial volume effects in this region due to the intermingling of other structures such as the bed nucleus of the stria terminalis. The superior boundary of the ventral striatum was defined by drawing a diagonal line from the ventral tip of the lateral ventricle to the ventral edge of the internal capsule and continuing to the ventral boundary of the striatum (at approximately 15 mm lateral to the midline). The inferior boundary was defined by the underlying white matter. The medial boundary was defined by the neighboring white matter in anterior slices and a vertical line descending from the ventral tip of the lateral ventricle on more posterior slices.

Because some researchers prefer to divide the dorsal striatum into functional domains, we additionally created ROIs for the associative and sensorimotor sectors of the dorsal striatum in order to verify that results were not substantially influenced by the choice of structural vs. functional divisions of the dorsal striatum. These ROIs were performed following the procedures described in Martinez et al. (2003) in which the associative striatum is comprised of the dorsal caudate and the portion of the putamen lying anterior to the anterior commissure, while the sensorimotor striatum is comprised of the dorsal putamen posterior to the anterior commissure (see Supplementary Fig. 2).

The amygdala and hippocampus were traced on coronal slices. In order to minimize contamination from the higher BP_{ND} of the striatum, the most superior aspects of the amygdala (including all of the extended amygdala) and the hippocampus were excluded from the ROIs defining the amygdala and hippocampus. Additionally, the most posterior aspects of the amygdala and anterior aspects of the hippocampus were excluded from the amygdala and hippocampus ROIs, respectively, in order to limit the amount of contamination between the two neighboring structures.

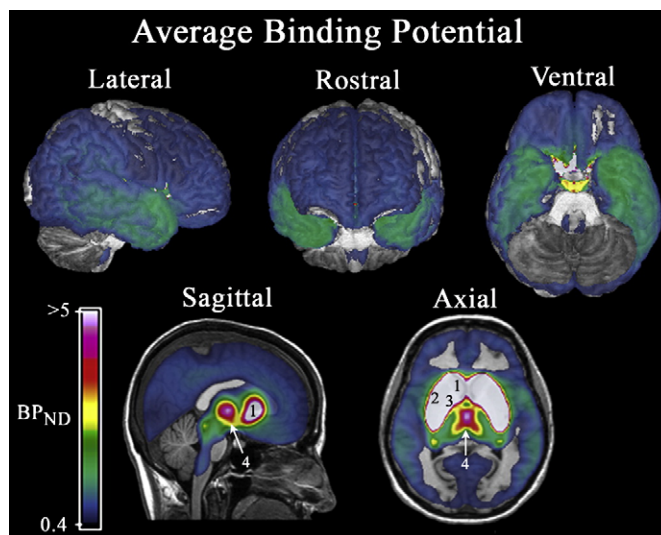


Fig. 1. Average [^{18}F]fallypride BP_{ND} . The data represent the average of all 45 subjects who participated in the present study. The data were thresholded to only show voxels with an average $BP_{ND} \geq 0.4$. The BP_{ND} maps were overlaid on (top) cortical surface renderings or (bottom) sagittal and axial slices of a template brain. Note that the selected color scale emphasizes regional differences in BP_{ND} within cortical areas at the expense of viewing differences in the basal ganglia regions. Because the caudate, putamen, ventral striatum, and globus pallidus all possess $BP_{ND} > 5$, it is not possible to distinguish their boundaries with this color scale. In addition to cortical areas, the sagittal slice in the second row shows a band of binding along the midline of the dorsal aspect of the brainstem, which includes the colliculi, the raphe nucleus, and the nucleus of the solitary tract, all of which have previously been identified to possess D2 receptors in autoradiographic studies (Yokoyama et al., 1994; Hurd et al., 2001). Number labels: (1) caudate, (2) putamen, (3) globus pallidus, (4) thalamus.

Table 1
BP_{ND} for select ROIs.

Area	Mean (S.D.)	Range	Volume of region (mm ³) [*]
Dorsal striatum	28.58 (4.02)	19.70–36.27	7129
Ventral striatum	20.30 (4.09)	8.94–28.06	1164
Medial thalamus [†]	2.52 (0.40)	1.43–3.16	3293
Lateral thalamus [†]	2.01 (0.33)	1.37–2.94	6246
Amygdala	2.01 (0.28)	1.37–2.52	2964
DA midbrain	1.96 (0.23)	1.48–2.47	756
Hippocampus	1.39 (0.24)	0.98–1.96	4422
Inferior lateral temporal [†]	1.25 (0.21)	0.79–1.61	36,531
General cortex defined by component 1 [†]	0.86 (0.17)	0.47–1.09	158,392
Medial frontal [†]	0.58 (0.11)	0.34–0.86	9671

* Note: volumes of anatomically defined ROIs are smaller than the true volumes of the structures due to the conservative nature of ROI definitions (see Materials and methods).

[†] Indicates ROI was delineated based on Component Loadings from the PCA of the z-transformed data, rather than anatomical definitions (see Materials and methods for details). Thresholds for the boundaries of these specific ROIs are described in the text.

With the current PET imaging techniques, the SN is visible in the DA midbrain region as two discrete foci of higher BP_{ND} (one per hemisphere), connected by a more medial region of lower intensity binding with the signal representing a combination of binding in the ventral tegmental area and contamination by the neighboring SN. Because of their small size and variability in precise positioning, it is not possible to draw an ROI of the DA midbrain at a single position for all subjects. Therefore, the DA midbrain was defined by drawing an ROI around the general area of the SN on 6 successive axial slices (resampled to 1-mm thickness), and then selecting all voxels above 40% of the maximum BP_{ND} within the region (an example of the resulting ROI for a subject is provided in Supplementary Fig. 3). The superior-most slice for the ROI was conservatively set at Talairach z = −7. Note that this resulted in the exclusion of the superior-most aspects of the SN, but this was deemed necessary because the scanner's resolution makes it difficult to distinguish signal arising from the top of the SN and signal arising from the overlying thalamus. This approach accurately labeled the visible foci in 43 of 45 subjects and was highly correlated with regions of interest drawn on individual subject's data prior to coregistration to a common space. The location of the other two subjects' SN was slightly shifted (several millimeters posterior, and 1–2 mm superior, respectively) and so the ROI was shifted accordingly. Because the SN ROI encompasses several different DA fields including the dorsal and ventral tier of the substantia nigra, the ventral tegmental area, and the retrorubral area, it is possible that subtle differences in ROI definition could affect the results. Post-hoc analyses in which we varied the ROI definition

parameters led to some subtle differences in correlation strength, with a focus on just the peak BP_{ND} voxels, or medial-most voxels tending to produce slightly higher correlations with the striatum, and slightly lower correlations with limbic regions than reported in the tables. However, the general pattern of correlations remained consistent with all areas showing significant correlations with the DA midbrain in Tables 1 and 2 remaining statistically significant and showing an identical rank ordering of their relative associations with the midbrain.

Five additional ROIs were defined based on the voxel-wise component loadings that emerged in Component 1 or 2 of the z-transformed PCA. We include these ROIs in order to fully characterize the component structure that emerged from the PCA. The ROI of cortex was defined as all areas with Component 1 loadings above 0.8 (which included most of parietal and lateral temporal cortex, as well as substantial portions of frontal cortex: areas in yellow in Fig. 3). The temporal and ventromedial prefrontal ROIs were defined by accepting all voxels within the respective regions with negative loadings on Component 2 of less than −0.2 and corresponds to the areas in blue in Fig. 4. The posterior-medial and anterior-lateral thalamic ROIs were defined by accepting all voxels within the thalamus that had loadings >0.2 or <−0.2, respectively, on Component 2, which corresponds to the two thalamic regions displayed in Fig. 4.

Results

Analysis of raw BP_{ND}

Table 1 displays the mean, standard deviation, and range of BP values in selected ROIs. PCA on the raw (non-z-transformed) BP_{ND} data produced a single component that explained 97.8% of the variance in the data set (eigenvalue = 11.5). Substantial positive component loadings emerged throughout the entire extent of the striatum bilaterally (see Fig. 2). These data make evident that individual differences in striatal BP_{ND} are primarily expressed at the level of the whole striatum, as opposed to arising distinctly in the separate topographic areas that make up the striatum (e.g., caudate, putamen, nucleus accumbens). This was confirmed by ROI analyses, which revealed an extremely high correlation between the dorsal caudate and putamen ($r = 0.98, p < 1 \times 10^{-20}$): because of their high covariance we collapsed the dorsal caudate and putamen into a single ROI in all subsequent analyses. The ventral striatum also showed a substantial correlation with the dorsal striatum ($r = 0.93, p < 1 \times 10^{-20}$). Use of alternative functional divisions of the striatum did not alter this conclusion, as the ventral striatum, associative striatum, and sensorimotor striatum all showed correlations with each other of $r > .94, p < 1 \times 10^{-20}$. Thus, even though the ventral striatum has lower overall

Table 2
Correlations of BP_{ND} in select regions of interest.

	Cortex [†]	Medial frontal [†]	Inferior lateral temporal [†]	Dorsal striatum	Ventral striatum	Amygdala	Hippo-campus	Medial thalamus [†]	Lateral thalamus [†]
Medial frontal [†]	0.71 ***								
Inferior lateral temporal [†]	0.77 ***	0.71 ***							
Dorsal striatum	0.30 *	0.10	−0.09						
Ventral striatum	0.23	0.04	−0.22	0.93					
Amygdala	0.29	0.34 *	0.10	0.45 **	0.49 **				
Hippocampus	0.17	0.21	0.08	0.35 *	0.40 *	0.72 ***			
Medial thalamus [†]	0.30 *	0.12	0.06	0.69 ***	0.72 ***	0.41 *	0.32 *		
Lateral thalamus [†]	0.33 *	0.43 **	0.51 ***	−0.26	−0.43 **	0.10	0.02	−0.27	
DA midbrain	0.23	0.26	0.17	0.30 *	0.30 *	0.59 ***	0.56 ***	0.23	0.24

* $p \leq 0.05$.

** $p \leq 0.005$.

*** $p \leq 0.0005$.

[†] Indicates ROI was delineated based on Component Loadings from the PCA of the z-transformed data, rather than anatomical definitions (see Materials and methods for details).

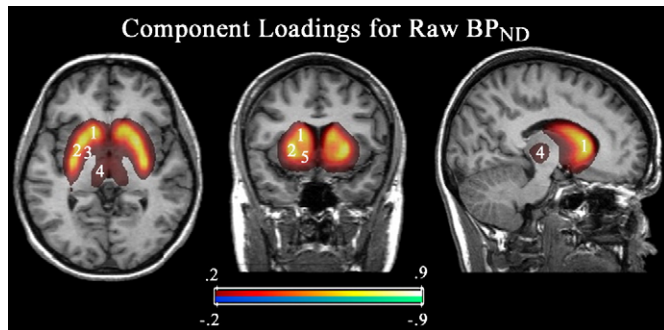


Fig. 2. Component loadings for the single component that arose from the raw BP_{ND} data. Strongly positive loadings emerged throughout the striatum, with highest loadings in the dorsal caudate and putamen, and slightly lower loadings in the ventral striatum. Outside of the striatum, only the globus pallidus and thalamus also loaded on this component but at much weaker levels than the striatum. The sagittal slice runs through the caudate and also displays part of the thalamus. In the present figure and all subsequent figures, the data were thresholded to only show component loadings ≥ 0.2 or ≤ -0.2 . Number labels: (1) caudate, (2) putamen, (3) globus pallidus, (4) thalamus, (5) ventral striatum.

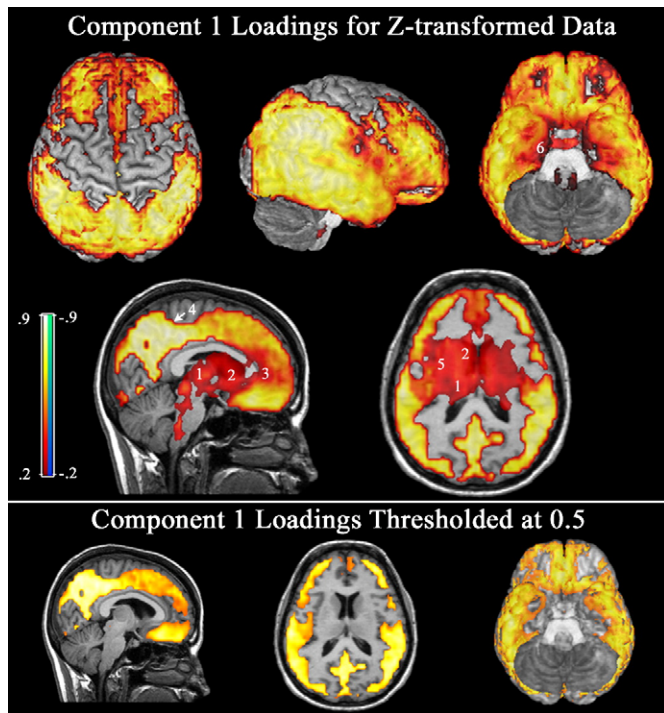


Fig. 3. Principal Component 1 from the z-transformed data. The 1st component is marked by a broad pattern of positive associations throughout widespread areas of the cortex. For purpose of display voxel-wise loadings are overlaid on surface renderings of the dorsal, lateral, and ventral surface of the brain (left to right top row), as well as a midline sagittal and an axial slice at the level of the dorsal striatum (2nd row). The strongest loadings localized to the posterior cingulate/precuneus region, with additional strong loadings in parietal cortex, anterior and ventral temporal cortex, and portions of the frontal lobe. The bottom of the figure shows the sagittal and axial slices and the ventral surface rendering after thresholding to only show loadings > 0.5 in order to more clearly delineate areas with strong loadings vs. areas with more moderate loadings. Although positive loadings were broad, several areas show only modest or moderate loadings on the 1st component, including the pregenual cingulate region and inferomedial temporal cortex (which drop out in the thresholded images). Moderate positive loadings can also be seen in the thalamus and striatum, which also drop out when thresholding is applied. Similarly, the sagittal slice in the 2nd row shows moderate loadings in the dorsal aspect of the brainstem (posterior pons), where binding occurred in the vicinity of the raphe nuclei, nucleus of the solitary tract, and locus coeruleus but did not surpass the 0.5 threshold. Number labels: (1) thalamus, (2) caudate, (3) pregenual cingulate, (4) precuneus, (5) putamen, (6) medial temporal cortex.

BP_{ND} than dorsal striatal regions individual differences are expressed in common across these areas. Outside of the striatum, only the medial thalamus (which has the highest level of D2-like BP_{ND} after the striatum) showed a clear, albeit weak loading on this component (max loading = 0.12). As expected, given the relatively lower levels (and hence variance) of D2-like BP_{ND} in extrastratial areas, no substantial loadings emerged in cortical areas.

Analysis of z-transformed BP_{ND}

In order to control for the differences in BP_{ND} variance across brain regions, and to allow examination of the relationship between striatal and extrastratial regions, all subsequent analyses were performed using z-transformed data. PCA of the z-transformed data revealed a complex picture of the relationship between D2-like binding in different brain regions. The first component (which accounted for 34.2% of the variance) involved broad areas of cortex (see Fig. 3), including both areas with modest level of D2 BP_{ND} as well as areas with more substantial cortical D2-like BP_{ND} . The highest loadings arose in posterior cortical regions including the precuneus, posterior cingulate, and portions of parietal cortex. Very high loadings also arose in lateral temporal cortical areas. In contrast, medial temporal regions had more modest loadings. Loadings in the frontal lobe were variable, with high levels arising along the gyrus rectus and in dorsolateral regions, and more moderate loadings along the medial wall and pregenual cingulate. Loadings in subcortical areas were consistently positive, but more modest than seen in cortex (mean = 0.35).

The second component (which explained 9.3% of the variance) involved strong positive loadings throughout the striatum (consistently 0.85 or above) and the globus pallidus (see Fig. 4). Positive loadings also emerged in the midline thalamus, especially its dorsal aspect. Modest positive loadings also emerged in the amygdala/hippocampus region.

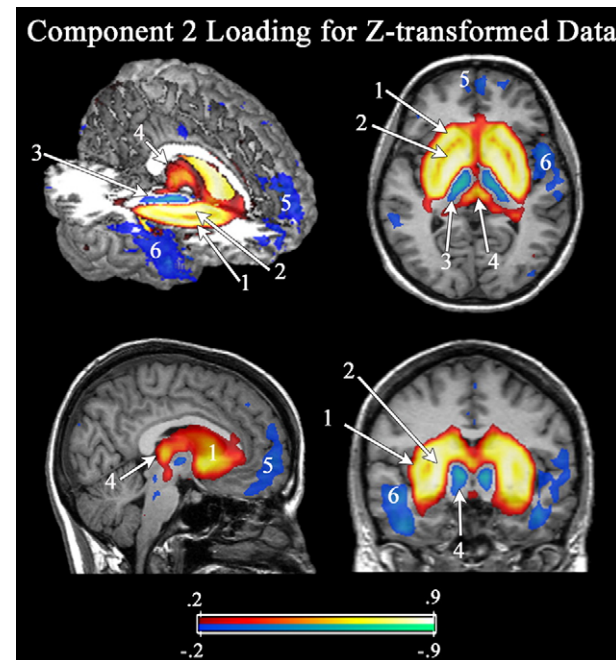


Fig. 4. Principal Component 2. The 2nd component involves strong positive loadings in the basal ganglia and moderate loadings in the posterior-medial thalamus and SN/VTA but negative loadings in the anterior-lateral thalamus and cortical regions. Number labels: (1) striatum, (2) globus pallidum, (3) anterior-lateral thalamus, (4) posterior-medial thalamus, (5) ventromedial PFC, (6) lateral temporal cortex, and (7) substantia nigra/ventral tegmental area.

Component 2 was also striking for the presence of negative loadings in several brain regions. A negative loading in this second component indicates that after controlling for the first component, the D2/D3 binding in a region was inversely related to the amount of binding in the striatum. In other words, the data suggest the presence of opposing influences on D2-like binding in the striatum and the areas with negative loadings. There were widespread negative loadings in the ventral and lateral temporal cortices. These negative loadings occurred bilaterally, although they appeared somewhat stronger in the left temporal pole and fusiform gyrus than the corresponding areas in the right hemisphere (with the strongest negative loading of -0.64 localizing to the left temporal pole). More modest negative loadings also arose throughout the medial wall of prefrontal cortex, particularly in ventromedial prefrontal cortex (Brodmann area 32, the medial portion of area 10, and area 14 along the gyrus rectus).

In order to further elucidate the association between the striatum and temporal areas showing strong negative loadings, we extracted BP_{ND} from an ROI containing all temporal lobe voxels with a Component 2 loading below -0.20 . Interestingly, whereas the cortex as a whole showed moderate associations with the dorsal striatum ($r=0.30$, $p<0.05$; see Table 2 for correlations between ROIs), these temporal areas showed no such association with striatal BP_{ND} ($r=-0.09$, $p>0.10$). After controlling for subject loadings on Component 1 (i.e., each subject's net score on the first component), a strong inverse association arose between these temporal regions and the dorsal striatum (partial $r=-0.60$, $p<0.00005$). This inverse association was even greater for the ventral striatum (partial $r=-0.70$, $p<0.0000001$). Because Component 1 heavily reflected cortical binding, we also ran the partial correlation analysis controlling for BP_{ND} limited to the broad swath of cortex that showed high (>0.80) loadings on Component 1 (Table 3). This analysis again revealed a strong inverse association between temporal cortical and striatal BP_{ND} (dorsal, $r=-0.54$; ventral, $r=-0.65$, both $p<0.0005$). These data indicate that there is a strong inverse relationship between temporal and striatal D2-like binding, after controlling for global cortical receptor availability.

Component 2 also revealed a marked dissociation between the medial/midline thalamus and more lateral aspects of the thalamus. Specifically, intense negative loadings emerged bilaterally in the lateral thalamus (loadings -0.60 to -0.72). In contrast, the midline/medial thalamus had positive loadings on this component. To further explore this apparent dissociation we defined ROIs based on the thalamic areas showing positive and negative loadings, respectively. This revealed markedly different patterns of correlation with the midline medial thalamus showing positive associations with the striatum, while the lateral thalamus showed a negative association. Differences also emerged in terms of other correlations, with the midline/medial thalamus showing significant correlations with the

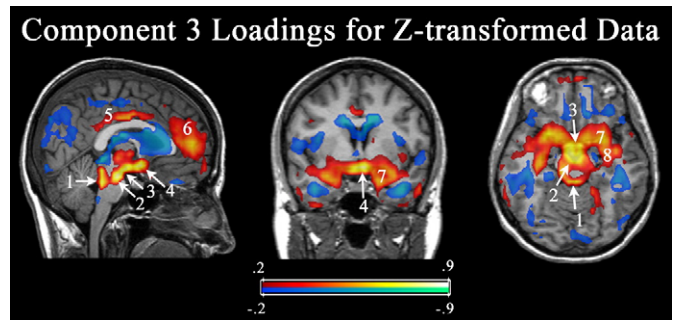


Fig. 5. Principal Component 3. The 3rd component produced its highest loadings in the DA midbrain, the mammillary bodies, and the hypothalamus. Note that in the coronal and axial slices a large area of the basal forebrain, including the extended amygdala also positively loads on this component. The axial slice passes through the mammillary bodies, which is slightly superior to the peak loadings in the substantia nigra/ventral tegmental area. Number labels: (1) colliculus/raphe, (2) substantia nigra/ventral tegmental area, (3) mammillary bodies, (4) hypothalamus, (5) posterior/mid-cingulate, (6) medial frontal cortex, (7) amygdala, and (8) hippocampus.

amygdala and hippocampus, while the lateral thalamus showed correlations with inferior and lateral temporal and medial frontal cortices.

The third component (4.8%) demarcated the DA midbrain (substantia nigra and ventral tegmental area: see Fig. 5). Given that this area is dominated by autoreceptors, it likely reflects a dissociable influence on autoreceptor levels. The component also loaded heavily on the hypothalamus and mammillary bodies, as well as extending posteriorly into a region that included the inferior colliculus, as well as the raphe, locus coeruleus, and nucleus of the solitary tract. Moderate to high loadings were also notable in the basal forebrain/extended amygdala, amygdala proper, and hippocampus. The emergence of the amygdala and hippocampus on the same component as the DA midbrain was not predicted but is consistent with the ROI analysis, which revealed a significant correlation between these structures and midbrain DA BP_{ND} ($r=0.59$ and $r=0.56$, respectively, both $p<0.0005$). Indeed, among all ROIs, the DA midbrain showed its strongest correlations with the amygdala and hippocampus, as seen in Table 2, and after controlling for Component 1 loadings in Table 3. In contrast to subcortical areas, there were few positive cortical loadings on Component 3, with the primary exception being parts of the cingulate, particularly the pregenual cingulate.

D2 receptor binding declines with age in both striatal and extrastriatal regions, and evidence suggests that the rate of decline varies between regions (Kaasinen et al., 2000; Reeves et al., 2002). Since only 4 of the 45 subjects were more than a decade above the mean of 24.4 years and no subjects were more than a decade below the mean age, it seems unlikely that the present results are an artifact of age. To further rule out this possibility, we reran the analysis, after

Table 3
Partial correlations controlling for Component 1 scores.

	Cortex [†]	Medial frontal [†]	Inferior lateral temporal [†]	Dorsal striatum	Ventral striatum	Amygdala	Hippocampus	Medial thalamus [†]	Lateral thalamus [†]
Medial frontal [†]	-0.39^*								
Inferior lateral temporal [†]	0.35^*	0.32^*							
Dorsal striatum	-0.35^*	-0.33^*	-0.60^{***}						
Ventral striatum	-0.37^*	-0.34^{***}	-0.71^{***}	0.92^{***}					
Amygdala	-0.30^*	0.10	-0.11	0.36^*	0.43^{**}				
Hippocampus	-0.34^*	0.04	-0.16	0.28	0.35^*	0.70^{***}			
Medial thalamus [†]	-0.33^*	-0.29^*	-0.35^*	0.64^{***}	0.69^{***}	0.31^*	0.25		
Lateral thalamus [†]	0.23	0.34^*	0.46^{**}	-0.42^{**}	-0.57^{***}	0.00	-0.05	-0.43^{**}	
DA midbrain	-0.24	0.06	-0.07	0.22	0.23	0.54^{***}	0.53^{***}	0.15	0.17

* $p \leq 0.05$.

** $p \leq 0.005$.

*** $p \leq 0.0005$.

[†] Indicates ROI was delineated based on Component Loadings rather than anatomical definitions (see Materials and methods for details).

Table 4

Eigenvalues and percentage of the variance explained by each component for the z-transformed data in the original analysis and after controlling for age or gender.

Component	Primary analysis		Controlling for age		Controlling for gender	
	Eigenvalue	Variance explained	Eigenvalue	Variance explained	Eigenvalue	Variance explained
1	14.99	34.19%	14.84	34.01%	14.94	34.23%
2	4.06	9.26%	4.06	9.30%	4.01	9.20%
3	2.09	4.77%	2.08	4.78%	2.08	4.75%

removing the effect of age. This had only minimal effects on the results (see Table 4) as the relative patterns remained the same and the amount of variance explained by the components only changed slightly. We similarly reran the analysis after controlling for gender. Again, this had minimal impact on the results. In order to test the stability of the component structure, we additionally performed a jackknife analysis (Shao and Tu, 1996), which demonstrated substantial stability in the observed component structure (see Supplementary data).

Discussion

In the present paper we applied the PCA strategy to reveal the spatial organization of D2-like BP_{ND} in the human brain. When multiple regions share high positive loadings on a given component, the loadings (and the corresponding correlations of ROIs) suggest there is a common influence explaining a portion of the variance. However, the data do not clarify the source of this influence, which could reflect fundamental biological processes, a methodological source of variance in the measurement of BP_{ND} , or both. In contrast, to the extent that areas show separate patterns of loadings, it suggests that the variances are caused by different influences, be they functional or methodological. As such, the results of the present analyses help identify which organizational features need to be explained and may suggest hypotheses regarding the functional or methodological influences that cause the spatial organization of D2-like BP_{ND} . In the discussion that follows we highlight the core organizational features that need to be explained, with the hope that it will lead to experimentation to directly test potential sources of influence across brain regions. We also note some critical methodological variables that may influence the observed patterns of BP_{ND} across subjects.

A key conclusion that arises from present analyses is that we cannot treat D2-like BP_{ND} measured only in the striatum as a global index of D2-like receptor status throughout the whole brain. The cortex and striatum largely loaded on separate components, and only 10% of the variance in overall cortical D2-like BP_{ND} was explained by striatal D2-like BP_{ND} . The relative dissociation between cortical and striatal regions appears to at least grossly conform to the classic distinction between nigrostriatal and mesocortical DA systems and suggests distinct regulatory influences on the target D2-like receptors of these two systems. Several factors may contribute to this differential regulation including differences in the transmission and termination of DA. For instance, DA released into the striatum is rapidly removed from the synapse, whereas in cortex, the low levels of DA transporter allow released DA to remain in the synapse for significantly longer periods of time (Seamans and Yang, 2004). Evidence for the separate regulation of cortical and striatal binding has also been observed for D1 receptor BP_{ND} (Abi-Dargham et al., 2002), which suggests that the observed independence of striatal and extrastriatal binding is a general feature of the DA system.

A methodological caveat is necessary in interpreting data on the modest relationship of striatal and extrastriatal BP_{ND} . Extracellular levels of DA are substantially higher in the striatum than in the cortex (Moghaddam et al., 1993), and this may differentially impact measures of receptor availability. The BP_{ND} of benzamides such as

[¹⁸F]fallypride are affected by endogenous DA levels (Riccardi et al., 2005, 2008). Because of this, BP_{ND} is interpreted as a measure of receptor availability, rather than absolute receptor density. It has been argued that endogenous DA leads to an average underestimation of BP_{ND} of 20–30% for D2 radioligands in the striatum (Laruelle, 2000; note that given existing data, [¹⁸F]fallypride is predicted to be slightly less susceptible to this underestimation than other striatal ligands, such as [¹¹C]raclopride). Endogenous DA appears to exert substantially less impact on cortical BP_{ND} , as demonstrated by the higher stability of cortical BP_{ND} in the face of pharmacological manipulations (Cropley et al., 2008; Okauchi et al., 2001; Riccardi et al., 2005, 2008). Given the observation of different sensitivity to endogenous DA, as well as differences in DA cell firing, metabolism, and turnover across nigrostriatal, mesolimbic, and mesocortical regions (Bannon and Roth, 1983), it is possible that some of the observed differences in striatal vs. extrastriatal BP_{ND} could arise from regional differences in extracellular DA or the regulation of DA release as opposed to specific differences in receptor density or affinity. Unfortunately, at present it is not possible to fully tease apart the differential contributions to observed BP_{ND} using *in vivo* PET. It may, however, be possible with animal studies and human post-mortem studies to determine the relative contribution of receptor concentration, receptor affinity, and presynaptic or metabolic effects on these regional patterns of receptor availability.

The PCA of z-transformed data identified specific areas of cortex that show unique associations with striatal BP_{ND} . Of note, Component 2 revealed an inverse association between BP_{ND} in ventral and lateral temporal cortex and the striatum after controlling for the first (cortical) component. Critically, this negative relationship was only clearly visible after controlling for the first (largely cortical) component. This suggests that there is an inverse interaction between D2-like BP_{ND} in the temporal cortex and striatum, but that it may be obscured unless one controls for other global influences on D2-like receptor availability. A more modest inverse relationship was also observable along the medial frontal wall (particularly ventrally). While preclinical models have described inverse relations between DA functioning in frontal and striatal regions (Deutch, 1992; Pycock et al., 1980; Weinberger, 1987), far less attention has been paid to the temporal cortex. One exception is medial temporal regions, which have been found to regulate aspects of striatal DA functioning (Heinz et al., 1999; Louilot and Choulli, 1997). However, to our knowledge, no existing data specifically addresses cross-regulation between DA receptor functioning in the striatum and more lateral temporal cortical areas.

A striking aspect of this study was the extent to which areas that are in close proximity often showed very different patterns of component loadings. For instance, subcortical medial temporal structures showed substantially different relationships than more lateral temporal areas, potentially reflecting a mesolimbic vs. mesocortical projection system. The separation between different parts of the thalamus was particularly striking, with more medial/midline and lateral thalamic regions demonstrating opposite loadings on some components. The thalamus shows substantial nuclei-specific heterogeneity in the DA cell groups from which it receives projections and in its level of D2, D3, and DA transporter expression (Garcia-Cabezas et al., 2007; Rieck et al., 2004; Sanchez-Gonzalez et al., 2005).

There are marked differences in BP_{ND} levels across thalamic nuclei, with the highest levels corresponding to the rostral half of the dorsal midline thalamic nuclei (including paraventricular and parataenial nuclei) and lower levels in more lateral structures (Rieck et al., 2004). The PCA appears to be capturing this distinction, suggesting that the midline thalamic nuclei with higher BP_{ND} are regulated differently than the more laterally located nuclei with lower BP_{ND}. The observation of nuclei specific influences of D2-like binding is of particular interest for schizophrenia, in that recent studies have indicated the presence of lowered [¹⁸F]fallypride BP_{ND} in schizophrenic patients (Buchsbaum et al., 2006; Kessler et al., 2009). The present data suggest the potential utility of distinctly analyzing medial and lateral thalamic regions in future studies of thalamic DA. Indeed, the data suggest caution in applying a thalamic-wide ROI, which may obscure regionally or nuclei-specific effects.

Whereas different parts of the thalamus showed dissociable loadings, the striatum (as well as the globus pallidum) showed an extremely homogenous pattern of component loadings, with almost the entire variance accounted for by a single component in the raw analysis of BP_{ND}. An important methodological factor that could increase homogeneity in this area is contamination of counts from neighboring areas of the striatum. However, the level of observed covariance between dorsal (caudate/putamen, or associative/sensorimotor) and ventral striatal regions far exceeds the amount of covariance that would be predicted simply based on a contamination of counts across striatal regions (Mawlawi et al., 2001). We note in this regard that we applied no additional smoothing to the data and provided a large gap between ventral striatum and caudate and putamen ROIs in order to minimize the contribution of neighboring voxels to both ROIs. Moreover, the homogenous component loadings spread across relatively distal areas of the striatum (areas that are 30 mm distant still show similar loadings). This contrasts with the thalamus, where areas that are only a few millimeters apart show dramatically different loadings.

The homogenous loadings of the striatum suggest a common influence over individual differences in D2-like BP_{ND} that cuts across different functional zones of the striatum. Indeed, although the ventral striatum (nucleus accumbens) is classically treated as part of the mesolimbic system rather than the nigrostriatal system, its pattern of loadings and correlations converged with the rest of the striatum, rather than with limbic areas. As such, individual differences in D2-like receptor availability are likely to produce similar impacts across a number of affective, cognitive, and motoric domains. This may lead to the common expression of certain cognitive, affective, or behavioral traits, despite each of the traits reliance on circuits involving different striatal regions.

The homogenous striatal loadings also imply that, at least in healthy individuals, variables that correlate with baseline D2-like BP_{ND} in one portion of the striatum will typically correlate with BP_{ND} in all areas of the striatum. This conclusion does not exclude the possibility that some areas of the striatum will show greater associations with a given trait than another region. However, true dissociations (as demonstrated by tests for significant differences between correlations) in the correlates of D2-like BP_{ND} across striatal regions are unlikely. Rather, correlations with different ROI regions are likely to all be in a similar direction, although some may reach an arbitrary level of statistical significance, while others fall below this significance level. For example, in a recent study by Volkow et al. (2006) in which striatal [¹¹C]raclopride binding was correlated with prefrontal and cingulate glucose metabolism in subjects with a positive history of alcoholism, correlations with the ventral striatal ROIs were always in the same direction as those for the dorsal striatal ROIs. In all cases where there was a highly significant correlation in a dorsal striatal ROI, there was also a significant correlation with the ventral striatal ROI. Only when effect sizes were more modest for the dorsal striatal ROIs did the ventral striatal ROI fail to produce similarly

statistically significant results, but this may be attributed to statistical power issues, and the arbitrary nature of a $p < 0.05$ cutoff, rather than a dissociation, since the correlations for the dorsal and the ventral striatal ROI were not significantly different.

The observed homogeneity in individual differences in striatal D2-like BP_{ND} also does not exclude regional variation in other measures of DA functioning (such as synthesis or release). Indeed, pharmacological studies of DA release increasingly indicate that DA release in different striatal regions is associated with different behavioral responses (Leyton et al., 2002; Clatworthy et al., 2009; Martinez et al., 2005). Taken together, these data raise the possibility that there are distinct sources of individual differences in striatal DA functioning, some of which, like D2 receptor availability occur at a rather global level, while others, like DA release, have more regionally specific effects. We note, however, that a true test of dissociation of regional differences in the functional correlates of DA release will require direct tests of significant differences in correlations in the same manner as we have suggested would be needed for measures of D2-like receptor availability.

A final feature of note relates to the identification of a distinctive component loading on the DA midbrain. Midbrain DA binding primarily reflects autoreceptors, particularly of the D2-short variety (Drukarch and Stoof, 1990; Khan et al., 1998; Sesack et al., 1994). The emergence of a specific component labeling this region suggests that there may be unique individual differences in autoreceptor expression that are dissociable from the more general influences on cortical and striatal DA levels. Interestingly, the amygdala–hippocampus, hypothalamus, and basal forebrain also showed high positive loadings on this component. The reason for this topographically specific covariance between these regions is currently unclear. It may be speculated that this link reflects autoreceptor expression as areas such as the amygdala are known to have potent terminal D2 autoreceptors (Bull et al., 1991), but data supporting or refuting such a hypothesis remain scarce.

Because [¹⁸F]fallypride binds at both D2 and D3 receptors, it is possible that the emergence of different components in the PCA could relate to the relative concentration of D2 vs. D3 receptors in different regions. In most cortical and subcortical regions, the D2 receptor is more abundantly expressed than the D3 receptor (Gurevich and Joyce, 1999; MeadorWoodruff et al., 1996), but the ratio of D2 to D3 receptor expression varies across regions. For instance, the density of D2 receptors is around six times greater than D3 densities in the dorsal caudate, but only around twice as plentiful in the basolateral amygdala and nucleus accumbens (Gurevich and Joyce, 1999). However, the present data appear inconsistent with a distinctive D3 component. Specifically, the ventral striatum did not show a distinct pattern relative to the dorsal striatum, despite these large differences in D2/D3 receptor ratios. Similarly, the amygdala and hippocampus showed very similar patterns and a high correlation despite evidence of significant D3 receptors in the amygdala but not the hippocampus (Murray et al., 1994).

A final source of methodological influence that might impact the results relates to morphological variability across subjects. This could come in to play in two respects. First, individual differences in grey matter volume or density could influence the corresponding amount of receptor sites. We have previously observed positive associations between grey matter volume and/or density in select cortical regions, and in the midbrain, thalamus, and striatum (Woodward et al., 2009). However, these are unlikely to explain the larger patterns observed in these analyses, in that cortically, the correlations between grey matter and BP_{ND} were regional specific, whereas Component 1 of the z-transformed data occupies most of the cortex. Similarly, although grey matter measures showed a correlation with BP_{ND} in the caudate, no association was observed for the putamen, whereas, both the raw and z-transformed analyses in the present study show similarity across all striatal regions. A second manner where morphological issues might impact the results is in misregistration of regions due to the use of template brains, and partial

volume averaging around the edges of structures with differing levels of D2-like receptors. We note, however, that such effects would likely produce patterns of association around the edges of structures (particularly smaller structures), but such effects were not readily apparent (the lateral thalamus is perhaps the only region where such an argument might be marshaled given the narrow band of component loadings in this region). Additionally, the large size of many of the regions with high component loadings (broad swaths of cortex, the striatum) and the correspondingly large ROIs contain enough voxels that individual differences at the edges of regions could not explain the larger pattern of associations.

To our knowledge, this is the first paper to attempt to apply a voxel-wise PCA strategy to understanding the spatial organization of individual difference in neuroreceptor binding. Such a strategy may prove beneficial for a range of different receptor systems and may capture relationships that would likely be missed using a small set of a priori ROIs. The results of such analyses have the potential to both generate novel hypotheses about the organization and cross-regulation of neurotransmitter systems and inform the design and interpretation of experiments with radioligands.

Acknowledgments

Funding for this research was provided by the National Institute of Drug Abuse (1R01 DA019670-02), the National Institute of Mental Health (5R01 MH60898-03 and 1R21 MH058757-01), and the National Science Foundation (#0332219). We dedicate this paper to the memory of Keith Worsely who provided advice on how to use his PCA_image software. We additionally thank Alain Dagher and Sylvain Milot of the Montreal Neurological Institute for advice in formatting data for the principal component analysis and using the MNI network. Conflict of interest statement: Dr. Robert M. Kessler holds a patent for the use of fallypride in humans, although there are no plans currently to market fallypride commercially.

Appendix A. Supplementary data

Supplementary data associated with this article can be found, in the online version, at doi:10.1016/j.neuroimage.2010.02.006.

References

- Abi-Dargham, A., Mawlawi, O., Lombardo, I., Gil, R., Martinez, D., Huang, Y.Y., Hwang, D.R., Keilp, J., Kochan, L., Van Heertum, R., Gorman, J.M., Laruelle, M., 2002. Prefrontal dopamine D1 receptors and working memory in schizophrenia. *J. Neurosci.* 22, 3708–3719.
- Bannon, M.J., Roth, R.H., 1983. Pharmacology of mesocortical dopamine neurons. *Pharmacol. Rev.* 35, 53–68.
- Buchsbaum, M.S., Christian, B.T., Lehrer, D.S., Narayanan, T.K., Shi, B., Mantil, J., Kemether, E., Oakes, T.R., Mukherjee, J., 2006. D2/D3 dopamine receptor binding with [¹⁸F]fallypride in thalamus and cortex of patients with schizophrenia. *Schizophr. Res.* 85, 232–244.
- Bull, D.R., Bakhtiar, R., Sheehan, M.J., 1991. Characterization of dopamine autoreceptors in the amygdala: a fast cyclic voltammetric study in vitro. *Neurosci. Lett.* 134, 41–44.
- Clatworthy, P.L., Lewis, S.J., Brichard, L., Hong, Y.T., Izquierdo, D., Clark, L., Cools, R., Aigbirhio, F.I., Baron, J.C., Fryer, T.D., Robbins, T.W., 2009. Dopamine release in dissociable striatal subregions predicts the different effects of oral methylphenidate on reversal learning and spatial working memory. *J. Neurosci.* 29, 4690–4696.
- Cropley, V.L., Innis, R.B., Nathan, P.J., Brown, A.K., Sangare, J.L., Lerner, A., Ryu, Y.H., Sprague, K.E., Pike, V.W., Fujita, M., 2008. Small effect of dopamine release and no effect of dopamine depletion on [¹⁸F]fallypride binding in healthy humans. *Synapse* 62, 399–408.
- Deutch, A.Y., 1992. The regulation of subcortical dopamine systems by the prefrontal cortex: interactions of central dopamine systems and the pathogenesis of schizophrenia. *J. Neural Transm.* 36 Suppl, 61–89.
- Drukarch, B., Stoof, J.C., 1990. D-2 Dopamine autoreceptor selective drugs—do they really exist? *Life Sci.* 47, 361–376.
- Farde, L., Suhara, T., Nyberg, S., Karlsson, P., Nakashima, Y., Hietala, J., Halldin, C., 1997. A PET-study of [¹¹C]FLB 457 binding to extrastriatal D2-dopamine receptors in healthy subjects and antipsychotic drug-treated patients. *Psychopharmacology (Berl.)* 133, 396–404.
- First, M.B., Spitzer, R.L., Gibbon, M., Williams, J.B., 1997. The structured clinical interview for DMS-IV (SCID-I). American Psychiatric Press, Inc., Washington, D.C.
- Friston, K.J., Frith, C.D., Liddle, P.F., Frackowiak, R.S., 1993. Functional connectivity: the principal-component analysis of large (PET) data sets. *J. Cereb. Blood Flow Metab.* 13, 5–14.
- Garcia-Cabezas, M.A., Rico, B., Sanchez-Gonzalez, M.A., Cavada, C., 2007. Distribution of the dopamine innervation in the macaque and human thalamus. *NeuroImage* 34, 965–984.
- Gardner, E.L., Ashby, C.R., 2000. Heterogeneity of the mesotelencephalic dopamine fibers: physiology and pharmacology. *Biobehav. Rev.* 24, 115–118.
- Garris, P.A., Wightman, R.M., 1994. Different kinetics govern dopaminergic transmission in the amygdala, prefrontal cortex, and striatum—an in-vivo voltammetric study. *J. Neurosci.* 14, 442–450.
- Gonzalez, R., Woods, R., 1992. Digital Image Processing, 3rd edition. Addison-Wesley Publishing Company, Reading, MA.
- Gurevich, E.V., Joyce, J.N., 1999. Distribution of dopamine D3 receptor expressing neurons in the human forebrain: comparison with D2 receptor expressing neurons. *Neuropsychopharmacology* 20, 60–80.
- Hall, H., Farde, L., Halldin, C., Hurd, Y.L., Pauli, S., Sedvall, G., 1996. Autoradiographic localization of extrastriatal D-2-dopamine receptors in the human brain using [¹¹C]epidepride. *Synapse* 23, 115–123.
- Heinz, A., Saunders, R.C., Kolachana, B.S., Jones, D.W., Gorey, J.G., Bacheviller, J., Weinberger, D.R., 1999. Striatal dopamine receptors and transporters in monkeys with neonatal temporal limbic damage. *Synapse* 32, 71–79.
- Hotelling, H., 1933. Analysis of a complex of statistical variables into principal components. *J. Educ. Psychol.* 27, 417–441.
- Hurd, Y.L., Suzuki, M., Sedvall, G.C., 2001. D1 and D2 dopamine receptor mRNA expression in whole hemisphere sections of the human brain. *J. Chem. Neuroanat.* 22, 127–137.
- Kaasinen, V., Vilkkman, H., Hietala, J., Nagren, K., Helenius, H., Olsson, H., Farde, L., Rinne, J., 2000. Age-related dopamine D2/D3 receptor loss in extrastriatal regions of the human brain. *Neurobiol. Aging* 21, 683–688.
- Kiebel, S.J., Poline, J.B., Friston, K.J., Holmes, A.P., Worsley, K.J., 1999. Robust smoothness estimation in statistical parametric maps using standardized residuals from the general linear model. *NeuroImage* 10, 756–766.
- Kessler, R.M., Whetsell, W.O., Ansari, M.S., Votaw, J.R., de Paulis, T., Clanton, J.A., Schmidt, D.E., Mason, N.S., Manning, R.G., 1993. Identification of extrastriatal dopamine D2 receptors in post mortem human brain with [¹²⁵I]epidepride. *Brain Res.* 609, 237–243.
- Kessler, R.M., Mason, N.S., Jones, C., Ansari, M.S., Manning, R.G., Price, R.R., 2000. [¹⁸F]N-allyl-5-fluoropropyl epidepride (fallypride): radiation dosimetry, quantification of striatal and extrastriatal dopamine receptors in man. *NeuroImage* 11 (6), s32.
- Kessler, R.M., Woodward, N.D., Riccardi, P., Li, R., Ansari, M.S., Anderson, S., Dawant, B., Zald, D., Meltzer, H.Y., 2009. Dopamine D2 receptor levels in striatum, thalamus, substantia nigra, limbic regions, and cortex in schizophrenic subjects. *Biol. Psychiatry* 65, 1024–1031.
- Kinahan, P.E., Rogers, J.C., 1989. Analytic 3D image reconstruction using all detected events. *IEEE Trans. Nucl. Sci.* 36, 964–968.
- Khan, Z.U., Mrzljak, L., Gutierrez, A., de la, C.A., Goldman-Rakic, P.S., 1998. Prominence of the dopamine D2 short isoform in dopaminergic pathways. *Proc. Natl. Acad. Sci. U.S.A.* 95, 7731–7736.
- Lammertsma, A.A., Bench, C.J., Hume, S.P., Osman, S., Gunn, K., Brooks, D.J., Frackowiak, R.S., 1996. Comparison of methods for analysis of clinical [¹¹C]raclopride studies. *J. Cereb. Blood Flow Metab.* 16, 42–52.
- Laruelle, M., 2000. Imaging synaptic neurotransmission with in vivo binding competition techniques: a critical review. *J. Cereb. Blood Flow Metab.* 20, 423–451.
- Lewis, D.A., Melchitzky, D.S., Sesack, S.R., Whitehead, R.E., Auh, S., Sampson, A., 2001. Dopamine transporter immunoreactivity in monkey cerebral cortex: regional, laminar, and ultrastructural localization. *J. Comp. Neurol.* 432, 119–136.
- Leyton, M., Boileau, I., Benkelfat, C., Diksic, M., Baker, H.F., Dagher, A., 2002. Extracellular dopamine, drug wanting, and novelty seeking: A PET/[¹¹C]raclopride study in healthy men. *Neuropharmacology* 41, 1027–1035.
- Louilot, A., Choulli, M.K., 1997. Asymmetrical increases in dopamine turn-over in the nucleus accumbens and lack of changes in locomotor responses following unilateral dopaminergic depletions in the entorhinal cortex. *Brain Res.* 778, 150–157.
- Maes, F., Collignon, A., Vandermeulen, D., Marchal, G., Suetens, P., 1997. Multimodality image registration by maximization of mutual information. *IEEE Trans. Med. Imag.* 16, 187–198.
- Martinez, D., Slifstein, M., Broft, A., Mawlawi, O., Hwang, D.R., Huang, Y., Cooper, T., Kegeles, L., Zarahn, E., Abi-Dargham, A., Haber, S.N., Laruelle, M., 2003. Imaging human mesolimbic dopamine transmission with positron emission tomography: Part II. Amphetamine-induced dopamine release in the functional subdivisions of the striatum. *J. Cereb. Blood Flow Metab.* 23, 285–300.
- Martinez, D., Gil, R., Slifstein, M., Hwang, D.R., Huang, Y., Perez, A., Kegeles, L., Talbot, P., Evans, S., Krystal, J., Laruelle, M., bi-Dargham, A., 2005. Alcohol dependence is associated with blunted dopamine transmission in the ventral striatum. *Biol. Psychiatry* 58, 779–786.
- Mawlawi, O., Martinez, D., Slifstein, M., Broft, A., Chatterjee, R., Hwang, D.R., Huang, Y., Simpson, N., Ngo, K., Van Heertum, R., Laruelle, M., 2001. Imaging human mesolimbic dopamine transmission with positron emission tomography: I. Accuracy and precision of D(2) receptor parameter measurements in ventral striatum. *J. Cereb. Blood Flow Metab.* 21, 1034–1057.
- Meador-Woodruff, J.H., Damask, S.P., Wang, J.C., Haroutunian, V., Davis, K.L., Watson, S.J., 1996. Dopamine receptor mRNA expression in human striatum and neocortex. *Neuropharmacology* 15, 17–29.
- Moghaddam, B., Berridge, C.W., Goldman-Rakic, P.S., Bunney, B.S., Roth, R.H., 1993. In vivo assessment of basal and drug-induced dopamine release in cortical and subcortical regions of the anesthetized primate. *Synapse* 13, 215–222.

- Mukherjee, J., Christian, B.T., Dunigan, K.A., Shi, B.Z., Narayanan, T.K., Satter, M., Mantil, J., 2002. Brain imaging of F-18-fallypride in normal volunteers: blood analysis, distribution, test-retest studies, and preliminary assessment of sensitivity to aging effects on dopamine D₂/D₃ receptors. *Synapse* 46, 170–188.
- Murray, A.M., Ryoo, H.L., Gurevich, E., Joyce, J.N., 1994. Localization of dopamine D₃ receptors to mesolimbic and D₂ receptors to mesostriatal regions of human forebrain. *Proc. Natl. Acad. Sci. U. S. A.* 91, 11271–11275.
- Okauchi, T., Suhara, T., Maeda, J., Kawabe, K., Obayashi, S., Suzuki, K., 2001. Effect of endogenous dopamine on endogenous dopamine on extrastriatal [¹¹C]FLB 457 binding measured by PET. *Synapse* 41, 87–95.
- Olsson, H., Halldin, C., Swahn, C.G., Farde, L., 1999. Quantification of [¹¹C]FLB 457 binding to extrastriatal dopamine receptors in the human brain. *J. Cereb. Blood Flow Metab.* 19, 1164–1173.
- Pearson, K., 1901. On lines and planes of closest fit to a system of points in space. *Philos. Mag.* 2, 557–572.
- Pluim, J.P.W., Maintz, J.B.A., Viergever, M.A., 2001. Mutual information matching in multiresolution contexts. *Image Vis. Comput.* 19, 45–52.
- Pyccock, C.J., Kerwin, R.W., Carter, C.J., 1980. Effect of lesion of cortical dopamine terminals on sub-cortical dopamine-receptors in rats. *Nature* 286, 74–77.
- Reeves, S., Bench, C., Howard, R., 2002. Ageing and the nigrostriatal dopaminergic system. *Int. J. Geriatr. Psychiatry* 17, 359–370.
- Rhode, G., Aldroubi, A., Dawant, B.M., 2003. The adaptive bases algorithm for intensity based non-rigid image registration. *IEEE Trans. Med. Imag.* 22, 1470–1479.
- Riccardi, P., Baldwin, R., Salomon, R., Anderson, S., Ansari, M.S., Li, R., Dawant, B., Bauernfeind, A., Schmidt, D., Kessler, R., 2008. Estimation of baseline dopamine D₂ receptor occupancy in striatum and extrastriatal regions in humans with positron emission tomography with [¹⁸F] fallypride. *Biol. Psychiatry* 63, 241–244.
- Riccardi, P., Li, R., Ansari, M.S., Zald, D., Park, S., Dawant, B., Anderson, S., Doop, M., Woodward, N., Schoenberg, E., Schmidt, D., Baldwin, R., Kessler, R., 2005. Amphetamine-induced displacement of [¹⁸F] fallypride in striatum and extrastriatal regions in humans. *Neuropsychopharmacology* 31, 1016–1026.
- Rieck, R.W., Ansari, M.S., Whetsell Jr., W.O., Deutch, A.Y., Kessler, R.M., 2004. Distribution of dopamine D₂-like receptors in the human thalamus: autoradiographic and PET studies. *Neuropsychopharmacology* 29, 362–372.
- Sanchez-Gonzalez, M.A., Garcia-Cabezas, M.A., Rico, B., Cavada, C., 2005. The primate thalamus is a key target for brain dopamine. *J. Neurosci.* 25, 6076–6083.
- Seamans, J.K., Yang, C.R., 2004. The principal features and mechanisms of dopamine modulation in the prefrontal cortex. *Prog. Neurobiol.* 74, 1–58.
- Seeman, P., Bzowej, N.H., Guan, H.C., Bergeron, C., Becker, L.E., Reynolds, G.P., Bird, E.D., Riederer, P., Jellinger, K., Watanabe, S., 1987. Human brain dopamine receptors in children and aging adults. *Synapse* 1, 399–404.
- Sesack, S.R., Aoki, C., Pickel, V.M., 1994. Ultrastructural localization of D₂ receptor-like immunoreactivity in midbrain dopamine neurons and their striatal targets. *J. Neurosci.* 14, 88–106.
- Shao, J., Tu, D., 1996. The Jackknife and Bootstrap. Springer-Verlag, New York.
- Thobois, S., Jahanshahi, M., Pinto, S., Frackowiak, R., Limousin-Dowsey, P., 2004. PET and SPECT functional imaging studies in Parkinsonian syndromes: from the lesion to its consequences. *NeuroImage* 23, 1–16.
- Tzschentke, T.M., 2001. Pharmacology and behavioral pharmacology of the mesocortical dopamine system. *Prog. Neurobiol.* 63, 241–320.
- Weinberger, D.R., 1987. Implications of normal brain development for the pathogenesis of schizophrenia. *Arch. Gen. Psychiatry* 44, 660–669.
- Wells III, W.M., Viola, P., Atsumi, H., Nakajima, S., Kikinis, R., 1996. Multi-modal volume registration by maximization of mutual information. *Med. Image Anal.* 1, 35–51.
- Williams, S.M., Goldman-Rakic, P.S., 1998. Widespread origin of the primate mesofrontal dopamine system. *Cereb. Cortex* 8, 321–345.
- Wise, R.A., 1996. Neurobiology of addiction. *Curr. Opin. Neurobiol.* 6, 243–251.
- Woodward, N.D., Zald, D.H., Ding, Z., Riccardi, P., Ansari, M.S., Baldwin, R.M., et al., 2009. Cerebral morphology and dopamine D₂/D₃ receptor distribution in humans: a combined [¹⁸F]fallypride and voxel-based morphometry study. *NeuroImage* 46, 31–38.
- Yokoyama, C., Okamura, H., Nakajima, T., Taguchi, J., Ibata, Y., 1994. Autoradiographic distribution of [³H]YM-09151-2, a high-affinity and selective antagonist ligand for the dopamine D₂ receptor group, in the rat brain and spinal cord. *J. Comp. Neurol.* 344, 121–136.
- Volkow, N.D., Wang, G.J., Begleiter, H., Porjesz, B., Fowler, J.S., Telang, F., Wong, C., Ma, Y., Logan, J., Goldstein, R., Alexoff, D., Thanos, P.K., 2006. High levels of dopamine D₂ receptors in unaffected members of alcoholic families: possible protective factors. *Arch. Gen. Psychiatry* 63, 999–1008.